SAND2015-7298J

Compatibility of a Conventional Non-aqueous Magnesium Electrolyte with a High Voltage V_2O_5 Cathode and Mg Anode

Niya Sa[1], Danielle L. Proffit[1], Albert L. Lipson[1], Miao Liu[3], Gopalakrishnan Sai Gautam[4], Nathan Hanh[5], Zhenxing Feng[1], Timothy T. Fister[1], Yang Ren[2], Cheng-Jun Sun[2], John T. Vaughey[1], Chen Liao[1], Paul A. Fenter[1], Kristin Persson[3], Gerbrand Ceder[4], Kevin R. Zavadil[5], Anthony K. Burrell[1]*

[1] Chemical Science and Engineering Division, Joint Center for Energy Storage Research, Argonne National Laboratory, Lemont, IL 60439, USA

[2] Advanced Photon Source, Argonne National Laboratory, Lemont, IL 60439, USA

[3]Environmental Energy Technology Division, Lawrence Berkeley National Laboratory, Berkeley, California 94720, USA

[4] Department of Materials Science and Engineering, Massachusetts Institute of Technology, Cambridge, MA 02139, USA

[5]Sandia National Laboratories, Albuquerque, NM 87185, USA

Correspondence and requests for materials should be addressed to Anthony K. Burrell (email: burrell@anl.gov)

Abstract

A major roadblock for magnesium ion battery development is the availability of an electrolyte that can deposit Mg reversibly and at the same time is compatible with a high voltage cathode. We report a prospective full magnesium cell utilizing a simple, non-aqueous electrolyte composed of high concentration magnesium bis(trifluoromethane sulfonyl)imide in diglyme, which is compatible with a high voltage vanadium pentoxide (V_2O_5) cathode and a Mg metal anode. For this system, plating and stripping of Mg metal can be achieved with magnesium bis(trifluoromethane sulfonyl)imide in diglyme electrolyte over a wide concentration range, however, reversible insertion of Mg into V_2O_5 cathode can only be attained at high electrolyte concentrations. Reversible intercalation of Mg into V_2O_5 is characterized and confirmed by X-ray diffraction, X-ray absorption near edge spectroscopy and energy dispersive spectroscopy.

Introduction

Development of high energy density rechargeable batteries is an important driving force in today's automobile industry. Although lithium-ion batteries (LIB) are widely used for energy storage in plug-in hybrid electric vehicles (PHEV), issues associated with manufacturing a cost-competitive battery of sufficient energy density have hindered their development for electric vehicle (EV) applications.[1] To achieve the highest energy density possible for commercial EV batteries, it would be advantageous to use a lithium-metal anode that results in a light and dense anode. However, lithium has a long history of undesirable behavior such as dendrite formation and the reactivity of Li metal with the electrolyte.[2] As scientists are still searching for

solutions to implement Li metal anodes, magnesium (Mg) has drawn considerable attention as an inexpensive earth-abundant metal that is potentially safer than lithium.[3,4] Mg shares many properties with lithium but has several potential advantages. First, Mg is the eighth most abundant element in the earth's crust reducing its cost to 4% of Li. Second, the theoretical electrochemical properties of Mg offer a reasonable alternative to Li, with a fairly low reduction potential of -2.37 V (*vs.* SHE) and a high theoretical volumetric capacity, 3833 mAh/cm^3 for Mg as compared to -3.04 V (*vs.* SHE) and 2046 mAh/cm^3 for Li.[5] Finally, Mg metal does not form dendrites during deposition, which makes it substantially safer than a Li metal anode.[6,7] Although a magnesium battery has been considered as a promising substitute for lithium based systems for some time, it is still at an early research stage with many challenges remaining. Studies have suggested that the formation of a surface layer at the Mg anode that blocks the diffusion of the Mg ion is the main impediment to achieve reversible magnesium deposition in many electrolytes.[8,9] The first breakthrough in the history of Mg electrolyte development was the discovery of organohaloaluminate based electrolytes which showed reversible Mg deposition/dissolution and were compatible with a Chevrel phase cathode (1.1 V *vs.* Mg).[3] Subsequently, significant effort was invested in the search for Mg electrolytes with a wider stability window that can reversibly plate and strip Mg. Many new electrolytes with improved stability were found, including magnesium organoborates[10,11] and various magnesium organohaloaluminate salts,[12] however, compatibility with high voltage cathodes is still problematic due to the strongly reducing characteristics of such electrolytes.

One of the biggest tasks is to devise a cell that uses a Mg metal anode with a high voltage intercalation cathode. While both high voltage cathodes and Mg metal anodes have been separately demonstrated, no electrolyte has been identified that is compatible with both electrodes. In particular, electrolytes that have shown reversible Mg plating and stripping are corrosive to metal oxides. A successful non-aqueous Mg electrolyte needs to avoid forming a passivation layer at the Mg anode, have high ionic conductivity, a high dielectric constant, be compatible with high voltage cathode materials, and exhibit high efficiency plating and stripping of the Mg metal. Here, we report a conventional electrolyte, $Mg(TFSI)_2$ in diglyme (abbreviated as $Mg(TFSI)_2$/DG), that is compatible with a Mg metal anode and a high voltage orthorhombic V_2O_5 cathode. This is the first report of a full cell configuration of a magnesium metal anode with a high voltage cathode. Results indicate that plating and stripping of Mg can be achieved at a wide concentration range, but that reversible Mg insertion into V_2O_5 only occurs at high concentrations. Mg intercalation into V_2O_5 was confirmed by X-ray diffraction (XRD), X-ray absorption spectroscopy (XAS), and energy dispersive X-ray spectroscopy (EDX).

Results and Discussion

Cyclic voltammetry (CV) was conducted to evaluate reversible Mg deposition of $Mg(TFSI)_2$/DG electrolyte at a magnesium anode. Figure 1a shows CV of $Mg(TFSI)_2$/DG at a Pt electrode with electrolyte concentrations range from 0.1 M to 1.5 M. Results show that plating and stripping of Mg can be achieved at a wide concentration range, from 0.1 M to 1.5 M. Peak current density for magnesium deposition and dissolution increases as electrolyte concentration increases from 0.1 M to 1.0 M. However, deposition/dissolution current density

decreases at 1.5 M, possibly due to ion pair formation, which lowers the total number of effective charge carriers.[13,14] Interestingly, the onset potential for deposition decreases as the concentration increases; for instance, deposition onset potential is -0.57 and -0.22 V at 0.1 M and 1.5 M respectively. This difference indicates that Mg deposition is more energetically favorable at higher electrolyte concentrations, which is possibly due to the lowered desolvation energy at high electrolyte concentrations.[15,16] On the other hand, magnesium dissolution in $Mg(TFSI)_2$/DG electrolyte is comparably difficult and requires an ~2 V higher potential than that needed to deposit Mg. It is likely that this over-potential is due to the formation of a surface layer at the $Mg(TFSI)_2$/DG and Mg anode interface.[8,9,17] Unlike complex organomagnesium based electrolytes in ethers, which are strongly reducing and yield nearly 100% columbic efficiency, the $Mg(TFSI)_2$/DG electrolyte reported here has ~30% Coulombic Efficiency **(**Figure S1, SI). The mechanism for reversible magnesium deposition in $Mg(TFSI)_2$/DG is not well understood at this time. It is possible that the diglyme solvent could be the critical factor to provide a well dissociated environment for Mg ions and therefore to facilitate the effective Mg deposition and dissolution. However, future studies are needed to explore the Mg deposition/dissolution mechanism.

To evaluate the compatibility of $Mg(TFSI)_2$/DG electrolyte with a high voltage oxide cathode material, the anodic stability of the electrolyte was investigated. Linear sweep voltammetry (LSV) was conducted on a Pt working electrode as shown in Figure 1b. Oxidation onset potential was determined to be 4.2 V *vs.* Mg/Mg^{2+} for $Mg(TFSI)_2$/DG electrolyte, which is comparable to that found previously.[18] Anodic stability of $Mg(TFSI)_2$/DG was found to be

concentration independent with, for instance, the same oxidation onset potential for 1.0 M and 0.1 M $Mg(TFSI)_2$/DG electrolytes. Having an electrolyte stability window larger than 4 V is a significant improvement compared to the organomagnesium based electrolytes, where the largest window *versus* magnesium metal was ~3.5 V.[19,20]

The ionic conductivity of $Mg(TFSI)_2$/DG was characterized by electrochemical impedance spectroscopy and its concentration dependence is shown in Figure 1c. Conductivity increases with concentration and reaches its peak value, 5.2 mS/cm, at 1.0 M and then decreases as concentration increases due to lower ionic mobility. $Mg(TFSI)_2$/DG displays a higher conductivity as compared with the reported organo-halide or organomagnesium based electrolytes, where the highest ionic conductivity is ~3 mS/cm.[21,22] The improved ionic conductivity makes $Mg(TFSI)_2$/DG attractive for battery applications, since higher ionic conductivity reduces the IR drop across the cell. Based on the conductivity and plating characteristics, 1.0 M $Mg(TFSI)_2$/DG was selected for full-cell tests.

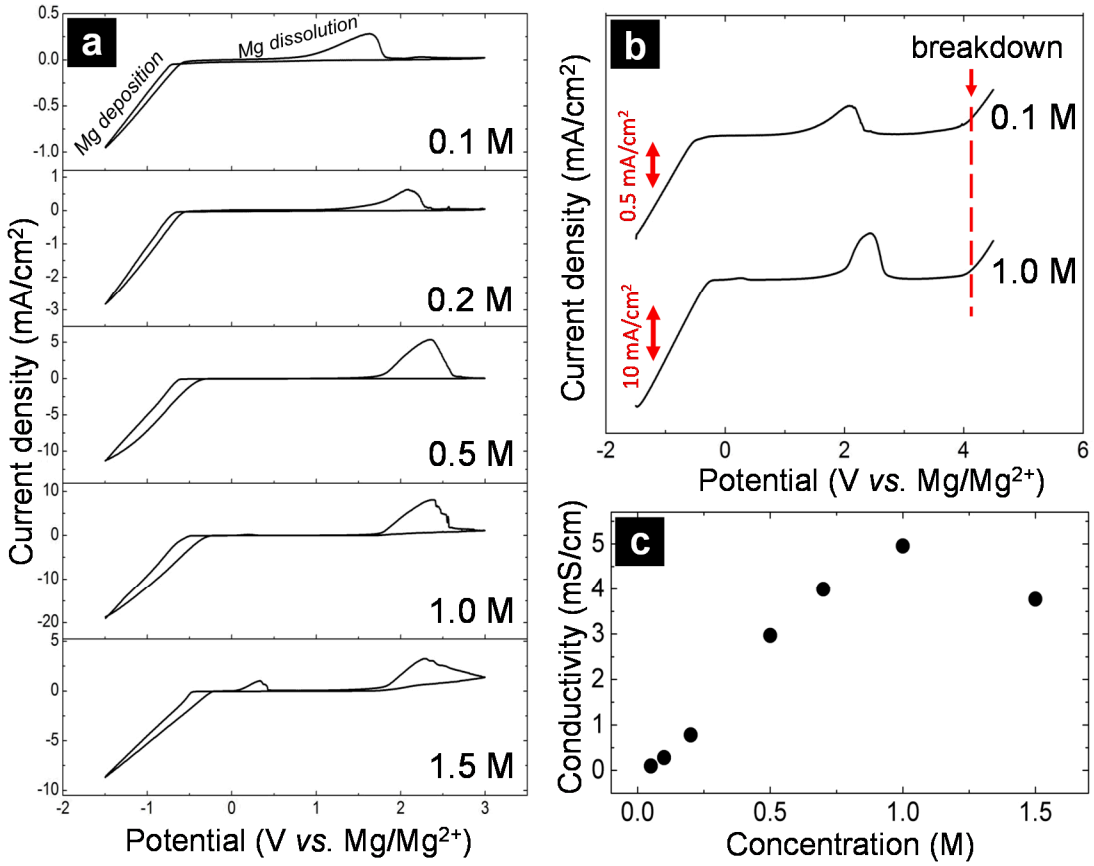

Figure 1. (a) Cyclic voltammograms (CV) of $Mg(TFSI)_2$/DG electrolyte at concentrations ranging from 0.1 M to 1.5 M. **(b)** Linear sweep voltammetry (LSV) of 0.1 M $Mg(TFSI)_2$/DG and 1.0 M $Mg(TFSI)_2$/DG electrolyte. For the CV and LSV measurements, a Pt disk was applied as the working electrode and a Mg ribbon was used as reference and counter electrode. Scan rate was set at 25 mV/sec. **(c)** Plot of the concentration dependence of the ionic conductivity for $Mg(TFSI)_2$/DG electrolyte.

Having established a clear understanding of the electrochemical performance of the $Mg(TFSI)_2$/DG electrolyte, we sought to demonstrate its potential application at a high voltage cathode using orthorhombic vanadium pentoxide (V_2O_5). A conventional coin cell composed of

a V_2O_5 cathode, 1.0 M $Mg(TFSI)_2$/DG electrolyte, and a magnesium metal anode was constructed to test the cycling performance. V_2O_5 was selected as the cathode material due to its reported intercalation with Mg ions which has been studied since the late 1980s.[23,24] However, those studies were limited to $Mg(ClO_4)_2$ based electrolytes,[25-27] which are not compatible with a metallic magnesium anode and likely contained significant amounts of water. Galvanostatic cycling of the coin cell using $Mg(TFSI)_2$/DG electrolyte demonstrated reversible cycling behavior, as shown in Figure 2a, with a 1st cycle discharge capacity of 82 mAh/g. The capacity was stable from the 2nd to the 10th cycles at 56 mAh/g with a Coulombic Efficiency of 65%. The capacity loss is possibly due to both sluggish kinetics for magnesium intercalation and the film formation at the magnesium anode. Two voltage plateaus at 2.1 V and 2.6 V *vs.* Mg/Mg^{2+} are observed from the galvanostatic charging data and are in good agreement with the theoretically predicted intercalation potentials from the Materials Project[28] for V_2O_5, while accounting for the charging overpotential (Figure S2, SI). Figure 2b presents the typical charge-discharge behavior for the $Mg(TFSI)_2$/DG system in terms of capacity versus cycle number, which shows no significant capacity fade after the 3rd cycle. Typical slow scan cyclic voltammograms using a three electrode setup, with V_2O_5 as the cathode and Mg disks as the reference and counter electrodes, were performed to confirm the two electrode coin cell cycling results. Two oxidation peaks were observed at 2.3 and 2.8 V, presented in Figure 2c, which is in good agreement with the plateaus of the charge-discharge curve. A reduction peak was observed at -0.5 V, with this large overpotential likely resulting from a passivating layer forming both on V_2O_5 and Mg anode in $Mg(TFSI)_2$/DG electrolyte. Potential correction for the Mg reference electrode is done by adding the redox molecule, ferrocene, to the $Mg(TFSI)_2$/DG

electrolyte (see Figure S3 and SI for detailed discussion). Cyclic voltammetry results indicate a 1.0 V potential shift to the lower value in $Mg(TFSI)_2$/DG electrolyte for the Mg metal reference electrode. In addition, galvanostatic cycling of coin cells with V_2O_5 as cathode and high surface area carbon as the anode was carried out to confirm the consistency of the cycling performance, with similar plateaus and voltage profiles observed (Figure S4, SI).

A noteworthy finding is that a relatively high electrolyte concentration is required in order for the intercalation/deintercalation reactions to occur at the cathode. Cycling using low concentration $Mg(TFSI)_2$/DG causes the cell to fail before it reaches a low discharge potential (Figure S5), however, cells with high concentrations of $Mg(TFSI)_2$, *i.e.* > 1.0 M, survive these conditions. This difference is possibly caused by $Mg(TFSI)_2$ coordinating with all the diglyme solvent at high concentrations, thereby minimizing the likelihood of oxidizing the solvent.[15] Another possibility is that at high electrolyte concentrations, electrical polarization at the electrolyte-cathode interface is reduced, which facilitates the diffusion of Mg into the cathode.

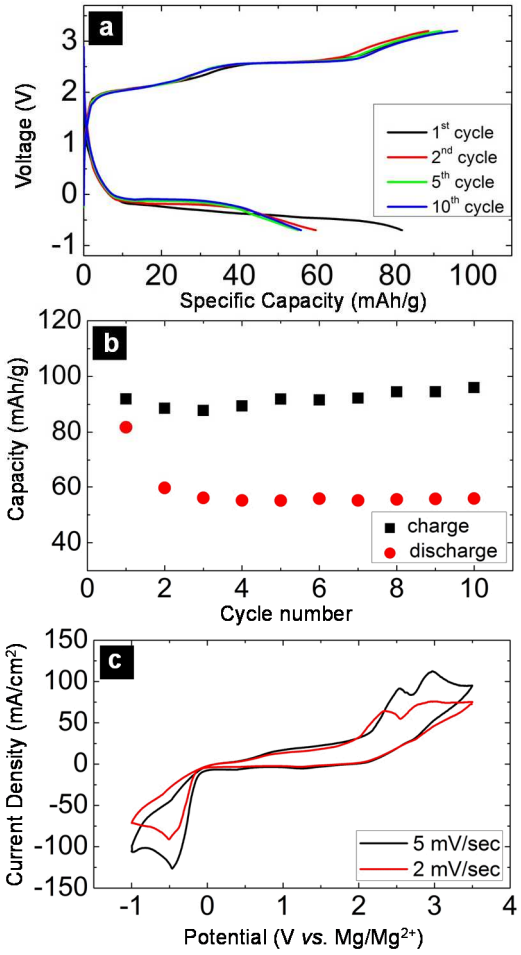

Figure 2. Characterization of the performance of a V_2O_5 cathode in the 1.0 M $Mg(TFSI)_2$/DG electrolyte: **(a)** First 10 cycles of galvanostatic charge-discharge curves for V_2O_5 against a Mg disk anode at a constant current of 20 µA; **(b)** Discharge and charge capacities of the two electrode coin cell versus cycle number; and **(c)** Slow scan cyclic voltammetry of V_2O_5 versus Mg as counter and reference electrode at a sweep rate of 5 mV/sec (black) and 2 mV/sec (red).

Mg intercalation was confirmed through changes of the vanadium (V) oxidation state in pristine, charged, and discharged V_2O_5 using XAS in transmission mode (see SI for details). Normalized vanadium K edge spectra and the Fourier Transform (FT) of k^2-weighted extended

XAS fine structure is shown in Figure 3. As expected, the vanadium X-ray absorption near edge spectroscopy (XANES) changed upon magnesium insertion. Discharged V_2O_5 (red) shows a ~0.8 eV edge shift (calculated by the first derivative of the normalized energy) of the main line towards lower energy, along with a 0.27 eV shift of the pre-edge peak toward lower energy. This change indicates a partial reduction of the V oxidation state upon magnesium intercalation.[29] The asymmetry of the pre-edge and reduction in fine structure in the near-edge region indicates a mixture of reduced and pristine vanadium states. The V_2O_5 pre-edge peak energy in the charged state shifted back to higher energy upon discharge, suggesting an increase of the vanadium oxidation state and reversibility of magnesium insertion into V_2O_5.[29] A reduction of pre-edge intensity for both charged and discharged states is possibly due to the distortion of the square pyramidal coordination of V^{5+} with the nearby five oxygen atoms since the pre-edge peak is considered to be a fingerprint that reflects the global symmetry around the V ions.[30,31] However, the edge position and intensity for the charged state did not completely recover back to the pristine state (0.06 eV difference), which can be ascribed to the incomplete extraction of Mg. The Fourier-transformed (FT) extended X-ray absorption fine structure (EXAFS) is shown in Figure 3b. The decrease in intensity of the first and second FT peaks reflects the structural disorder intrinsic to heterogeneous Mg insertion. EXAFS suggests that the V_2O_5 lattice structure remains unchanged after cycling. The nearly complete reversibility of the local atomic structure following charging is further evidence of reversible Mg intercalation in V_2O_5 through an intercalation pathway.

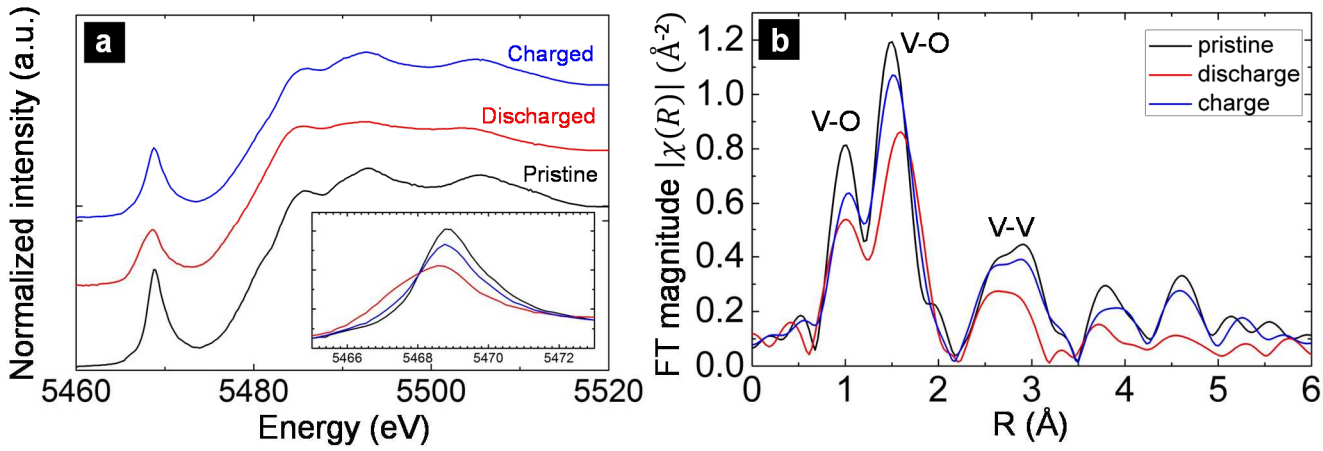

Figure 3. X-ray absorption characterization of the V_2O_5 cathode: **(a)** XANES spectra for pristine (black), charged (blue), and discharged (red) V_2O_5 at the vanadium k-edge; **(b)** the Fourier transform of the extended fine structure of pristine, charged, and discharged V_2O_5 at the vanadium K-edge. The spectra have not been phase-shifted.

To understand the structural changes of V_2O_5 upon Mg intercalation, synchrotron XRD was performed for orthorhombic V_2O_5 at pristine, charged and discharged states at various potentials, as shown in Figure 4. Diffraction for the pristine electrode shows peaks corresponding to the orthorhombic V_2O_5 structure (Pmmn, code 00-001-0359).[32] Magnesium insertion into V_2O_5 results in the formation of four new peaks, indicated by an asterisk "*" next to the new diffraction peaks. This phase transition occurs during the two plateaus while cycling galvanostatically, or equivalently at the oxidation/reduction peaks observed in the slow scan cyclic voltammetry. Two of the new peaks, observed at 18.044° and 25.544° during discharge, match with the (020) and (110) peaks of MgV_2O_5 ($Cmc2_1$, code 00-030-080).[33] The symmetry changes from Pmmn to $Cmc2_1$ upon Mg intercalation, indicating a layer sliding mechanism in

discharged $Mg_xV_2O_5$, where the $Mg_xV_2O_5$ phase possibly changes from α to ε phase (Figure S2, SI). First-principles calculation confirms that the α to ε phase transition is energetically favorable.[28] In contrast, the peaks at 14.711° and 13.399° corresponding to d-spacing of 6.02 Å and 6.60 Å could not be matched to any reported crystal structures and may correlate to the intercalated ε phase of V_2O_5, according to simulation, for which the diffraction pattern is shown (Figure S6, SI).

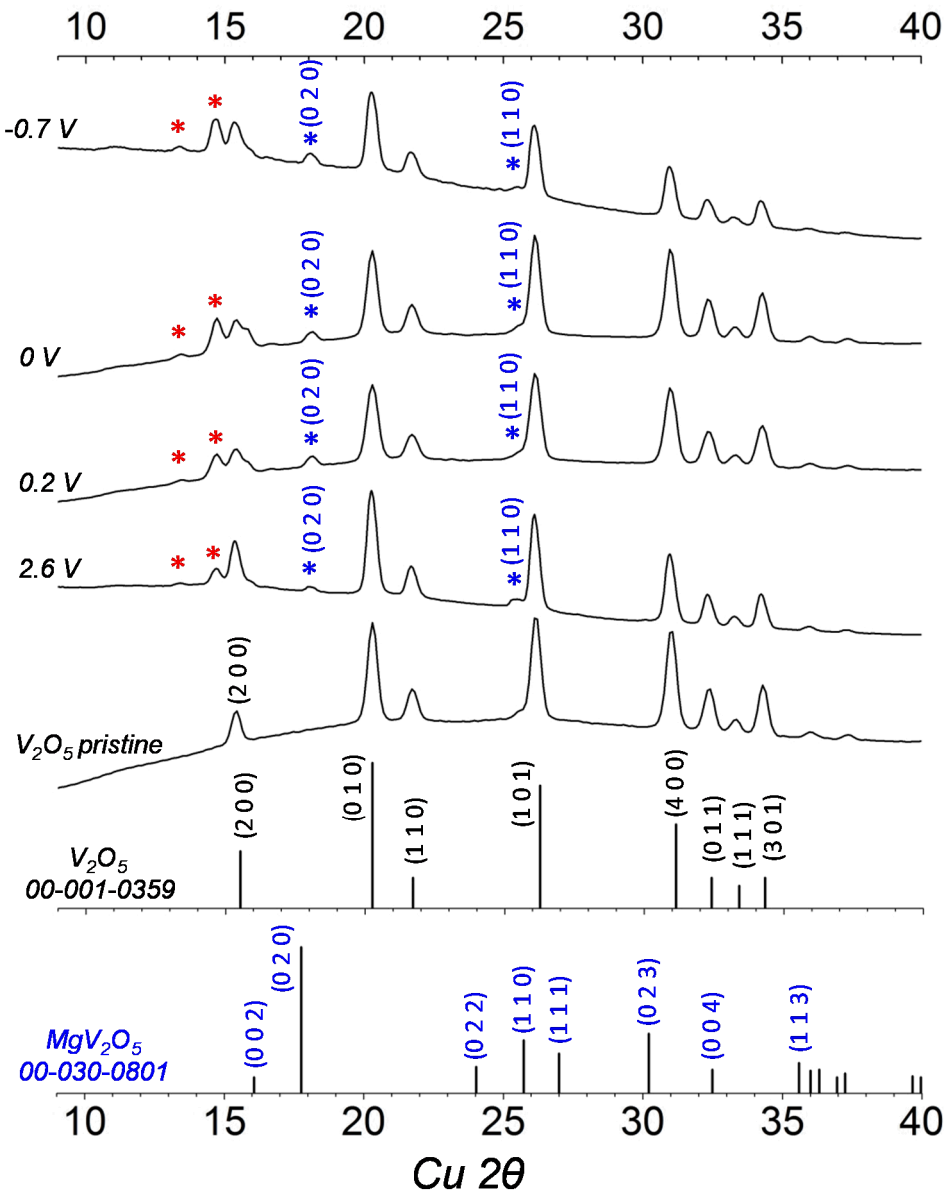

Figure 4. *Ex-situ* X-ray diffraction patterns for the pristine, discharged, and charged states of the V_2O_5 cathode. The bottom two profiles are XRD patterns from the ICDD PDF database for orthorhombic V_2O_5 and MgV_2O_5.

Surface morphology and chemical composition of the pristine V_2O_5, discharged V_2O_5 laminate, and cycled Mg anode were further characterized by Scanning Electron Microscopy

(SEM) and energy-dispersive X-ray spectroscopy (EDX). The V_2O_5 particle morphology showed no significant changes before and after discharging, as illustrated in Figure 5a and 5b. EDX was used to confirm the presence of Mg in the discharged V_2O_5 electrode. Figure 5c showed an increase in the characteristic peak of Mg for discharged V_2O_5 as compared to the charged and pristine V_2O_5, indicating a higher concentration of Mg. There is a small amount of Mg remaining in the charged V_2O_5, which could be due to surface film formation or the incomplete removal of Mg from V_2O_5. Surface morphology and elemental analysis for a Mg metal anode that was cycled 10 times versus V_2O_5 was also examined. The surface of the Mg anode appears reasonably smooth as shown in Figure 5d, however, upon closer inspection, shown in Figure 5e, there are pinholes that are hundreds of nanometers in diameter, which are possibly due to the stripping of Mg during cycling. EDX results suggest that nearly pure Mg is being deposited on the Mg anode during the plating process as shown in Figure 5f.

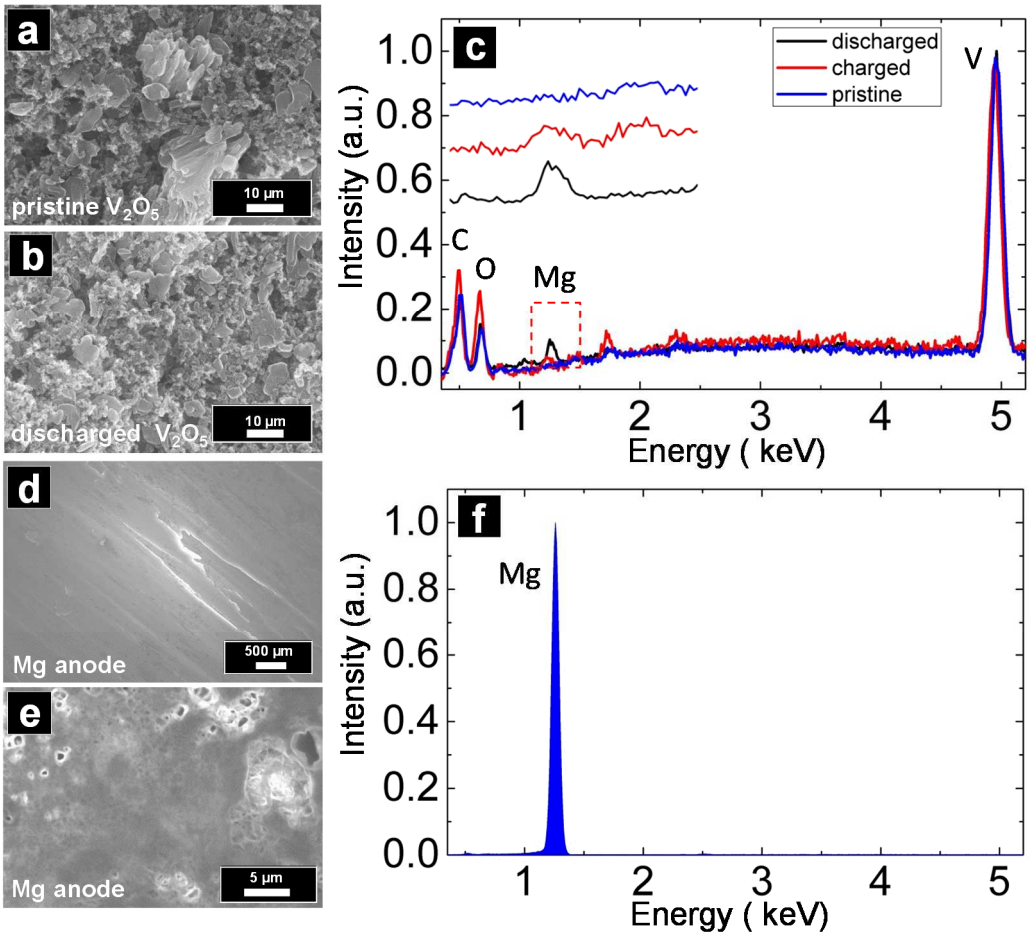

Figure 5. SEM and EDX characterization of the V_2O_5 cathode and Mg anode: **(a)** SEM image of pristine V_2O_5; **(b)** SEM of discharged V_2O_5; **(c)** Corresponding characteristic Mg spectrum from EDX for discharged (black), charged (red) and pristine (blue) V_2O_5. The inset shows the spectra from the boxed area in offset; **(d)** SEMs images of the cycled Mg anode at low magnification; **(e)** Cycled Mg anode at high magnification; **(f)** Corresponding Mg spectrum from EDX of the cycled Mg anode.

Conclusions

We have for the first time demonstrated a full cell Mg battery using a non-aqueous magnesium electrolyte, $Mg(TFSI)_2$/DG, that is compatible with both a high voltage V_2O_5 cathode and a magnesium metal anode. Electrochemical characterization suggests three promising characteristics for the $Mg(TFSI)_2$/DG electrolyte: (1) plating and stripping of Mg that can be achieved at a wide concentration range, from 0.1 M to 1.5 M; (2) anodic stability above 4.2 V *versus* Mg/Mg^{2+} and (3) high ionic conductivity, up to 5.2 mS/cm. The $Mg(TFSI)_2$/DG electrolyte in this Mg full cell reflects a compromise between the intermediate Coulombic Efficiency at the magnesium metal anode and compatibility with a high voltage cathode. Approximately 0.2 Mg was inserted per formula unit into V_2O_5, based on the obtained discharge capacity as compared with the calculated theoretical capacity (SI). Furthermore, the intercalation of Mg into V_2O_5 leads to the formation of MgV_2O_5, as well as another unidentifiable phase. While the cell suffers from a high overpotential and limited capacity at the cathode, it demonstrates the possibility of achieving full cell chemistry in a magnesium system. These findings suggest a potential path forward to creating a successful high voltage Mg battery. With an improved understanding of how this cell operates, new electrolytes and materials can be developed that show higher C oulombic Efficiency, capacity and voltage.

Methods

Preparation of the orthorhombic V_2O_5 cathode: Vanadium oxide electrodes were prepared by casting an 8:1:1 weight-ratio slurry of vanadium oxide (Fluka, > 99%), Timcal Super C45 carbon black, and polyvinylidene fluoride (PVDF) dissolved in N-methyl-2-pyrrolidinone (NMP) onto a 304 stainless steel current collector. These laminates were then dried at 75 °C in an oven for at least one hour before being punched as 7/16” diameter electrodes

Preparation of the $Mg(TFSI)_2$ in diglyme electrolyte: Magnesium bis(trifluoromethane sulfonyl)imide (99.5%, Solvionic, France) was dried in a vacuum oven at 170°C overnight before use. Diglyme (Aldrich, anhydrous, 99.5%) solvent was pretreated with molecular sieve (Aldrich, 3Å beads, 4-8 mesh) overnight and then added into the dried $Mg(TFSI)_2$. The as-prepared electrolyte was then stirred overnight before use.

Electrochemical measurements: Electrochemical Impedance Spectroscopy (EIS) is applied for electrolyte conductivity measurement. A home-built conductivity cell, fabricated with two platinum disks facing each other with 1 mm separation, is used for the EIS measurement. Conductivity cell is filled with electrolyte, and the frequency is scanned from 0.1 Hz to 100000 Hz. Impedance is calculated according to equation (1):

$$k = d/(A \cdot |\vec{z}|) \quad (1)$$

where *k* is ionic conductivity, *d* is the electrode distance, and *A* is the area of the electrode. Constant *d* and *A* are obtained by calibration of conductivity with standard KCl solution. A three electrode setup with a Pt disk as the working electrode (2 mm in diameter, CH instruments, Austin, TX) and polished Mg ribbon as the counter and reference electrode (99.9% purity, Sigma-Aldrich) is used to measure the cyclic and linear voltammagram of the electrolyte. Galvanostatic cycling of V_2O_5 *vs.* Mg in coin cells was performed using a Maccor series 4000 cycler at 20μA between -0.7 V and 3 V. A three electrode Swagelok cell configuration is used for the slow scan cyclic voltammetry measurement, with V_2O_5 on a stainless steel current collector as the working electrode, and a polished magnesium disk (7/16" diameter) as the counter and reference electrode. Electrochemical characterization was carried out using a multichannel potentiostat (Parstat MC, Princetion Applied Research, TN) under a pure argon atmosphere in a glove box where H_2O and O_2 level is kept under 1 ppm.

X-ray Diffraction: High energy X-ray diffraction (XRD) was carried out at Beamline 11-ID-C of the Advanced Photon Source (APS) at Argonne National Laboratory (ANL). The X-ray energy was 114.76 keV (corresponding to 0.10804 Å, the fixed wavelength for this station), which has a large penetration capability that allowed for the detection of structural changes of the bulk

material. The V_2O_5 powder was collected and sealed with kapton tape. An incident X-ray beam size of 0.5 mm × 0.5 mm was used. A Perkin Elmer area X-ray detector was used to collect the 2-dimensional diffraction patterns in transmission mode. The measured 2D diffraction patterns were calibrated using a standard CeO_2 sample and converted to one-dimensional intensity versus scattering angle patterns using Fit2D software.

X-ray absorption near edge structure (XANES): Ex-situ vanadium (V) K-edge X-ray absorption spectroscopy was performed to detect the change of the V valence states for charged and discharged cathodes at the beamline 20-BM-B at APS, Argonne National Lab. The measurements were carried out in transmission mode with a vanadium metal foil as a reference, which provides internal calibration for the X-ray energy. Coin cells with V_2O_5 as the cathode and Mg metal as the anode were cycled at constant current mode, 20 μA, for 10 cycles before holding at certain charged/discharged potentials. V_2O_5 powder was then collected and mixed homogeneously with cellulose at a mass ratio of 1:5 and pressed into pellets for the measurement. The XANES spectra were normalized and analyzed using the ATHENA software package. A full range XANES shown in Figure S6 indicates good normalization. The edge position, located at the maximum of the first derivative, was defined as 5465 eV.

Scanning Electron Microscopy (SEM) and Energy Dispersive X-ray Spectroscopy (EDX): Scanning electron microscopy and energy-dispersive X-ray spectroscopy characterization was performed using a Hitachi S4700-II scanning electron microscope equipped with an EDX detector mounted at a 30° take-off angle. Elemental composition was determined using a standardless ZAF (atomic number, absorption and fluorescence) corrected analysis. Both EDX and SEM were performed at an electron energy of 30 keV. Cathode materials collected from cycled coin cells were soaked and rinsed with acetone to remove any electrolyte residue on the surface prior to the EDX analysis.

References

1 Goodenough, J. B. & Park, K.-S. The Li-Ion Rechargeable Battery: A Perspective. *J. Am. Chem. Soc.* **135**, 1167-1176 (2013).
2 Orsini, F. *et al.* In situ Scanning Electron Microscopy (SEM) observation of interfaces within plastic lithium batteries. *J. Power Sources* **76**, 19-29 (1998).
3 Aurbach, D. *et al.* Prototype systems for rechargeable magnesium batteries. *Nature* **407**, 724-727 (2000).
4 Tarascon, J. M. & Armand, M. Issues and challenges facing rechargeable lithium batteries. *Nature* **414**, 359-367 (2001).
5 Yoo, H. D. *et al.* Mg rechargeable batteries: an on-going challenge. *Energy Environ. Sci.* **6**, 2265-2279 (2013).
6 Matsui, M. Study on electrochemically deposited Mg metal. *J. Power Sources* **196**, 7048-7055 (2011).
7 Ling, C., Banerjee, D. & Matsui, M. Study of the electrochemical deposition of Mg in the atomic level: Why it prefers the non-dendritic morphology. *Electrochim. Acta* **76**, 270-274 (2012).
8 Ratnakumar, B. V. Passive films on magnesium anodes in primary batteries. *J. Appl. Electrochem.* **18**, 268-279 (1988).
9 Lu, Z., Schechter, A., Moshkovich, M. & Aurbach, D. On the electrochemical behavior of magnesium electrodes in polar aprotic electrolyte solutions. *J. Electroanal. Chem.* **466**, 203-217 (1999).
10 Liebenow, C., Yang, Z. & Lobitz, P. The electrodeposition of magnesium using solutions of organomagnesium halides, amidomagnesium halides and magnesium organoborates. *Electrochem. Commun.* **2**, 641-645 (2000).
11 Mohtadi, R., Matsui, M., Arthur, T. S. & Hwang, S.-J. Magnesium Borohydride: From Hydrogen Storage to Magnesium Battery. *Angewandte Chemie-International Edition* **51**, 9780-9783 (2012).
12 Benmayza, A. *et al.* Effect of Electrolytic Properties of a Magnesium Organohaloaluminate Electrolyte on Magnesium Deposition. *J. Phys. Chem. C* **117**, 26881-26888 (2013).
13 Lee, D. K. & Allcock, H. R. The effects of cations and anions on the ionic conductivity of poly bis(2-(2-methoxyethoxy)ethoxy)phosphazene doped with lithium and magnesium salts of trifluoromethanesulfonate and bis (trifluoromethanesulfonyl)imidate. *Solid State Ionics* **181**, 1721-1726 (2010).
14 Rajput, N. N., Qu, X., Sa, N., Burrell, A. K. & Persson, K. A. The Coupling between Stability and Ion Pair Formation in Magnesium Electrolytes from First-Principles Quantum Mechanics and Classical Molecular Dynamics. *J. Am. Chem. Soc.* (2015).
15 McOwen, D. W. *et al.* Concentrated electrolytes: decrypting electrolyte properties and reassessing Al corrosion mechanisms. *Energy Environ. Sci.* **7**, 416-426 (2014).
16 Yoshida, K. *et al.* Oxidative-Stability Enhancement and Charge Transport Mechanism in Glyme-Lithium Salt Equimolar Complexes. *J. Am. Chem. Soc.* **133**, 13121-13129 (2011).
17 Mohtadi, R. & Mizuno, F. Magnesium batteries: Current state of the art, issues and future perspectives. *Beilstein Journal of Nanotechnology* **5**, 1291-1311 (2014).
18 Ha, S. Y. *et al.* Magnesium(II) Bis(trifluoromethane sulfonyl) Imide-Based Electrolytes with Wide Electrochemical Windows for Rechargeable Magnesium Batteries. *ACS Appl. Mater. Interfaces* **6**, 4063-4073 (2014).
19 Muldoon, J. *et al.* Electrolyte roadblocks to a magnesium rechargeable battery. *Energy Environ. Sci.* **5**, 5941-5950 (2012).
20 Guo, Y.-s. *et al.* Boron-based electrolyte solutions with wide electrochemical windows for rechargeable magnesium batteries. *Energy Environ. Sci.* **5**, 9100-9106 (2012).

21 Chusid, O. *et al.* Solid-state rechargeable magnesium batteries. *Adv. Mater.* **15**, 627-630 (2003).
22 Doe, R. E. *et al.* Novel, electrolyte solutions comprising fully inorganic salts with high anodic stability for rechargeable magnesium batteries. *Chem. Commun.* **50**, 243-245 (2014).
23 Wen-hai, Y., Da-zhi, W., Bin, Z., Shen-jun, W. & Li-xin, X. Insertion of bi-valence cations Mg 2+ and Zn 2+ into V 2O 5. *Solid State Commun.* **61**, 271-273 (1987).
24 Yu, W. H., Wang, D. Z., Zhu, B. & Zhou, G. E. Intercalation of Mg in V2O5. *Solid State Commun.* **63**, 1043-1044 (1987).
25 Novak, P., Imhof, R. & Haas, O. Magnesium insertion electrodes for rechargeable nonaqueous batteries - a competitive alternative to lithium? *Electrochim. Acta* **45**, 351-367 (1999).
26 Novak, P., Scheifele, W., Joho, F. & Haas, O. Electrochemical Insertion of magnesium into hydrated vanadium bronzes. *J. Electrochem. Soc.* **142**, 2544-2550 (1995).
27 Yu, L. & Zhang, X. G. Electrochemical insertion of magnesium ions into V2O5 from aprotic electrolytes with varied water content. *J. Colloid Interface Sci.* **278**, 160-165 (2004).
28 Jain, A. *et al.* Commentary: The Materials Project: A materials genome approach to accelerating materials innovation. *Apl Materials* **1** (2013).
29 Giorgetti, M. *et al.* In situ X-ray absorption spectroscopy characterization of V2O5 xerogel cathodes upon lithium intercalation. *J. Electrochem. Soc.* **146**, 2387-2392 (1999).
30 Wong, J., Lytle, F. W., Messmer, R. P. & Maylotte, D. H. K-edge absorption-spectra of selected vanadium compounds. *Phy. Rev. B* **30**, 5596-5610 (1984).
31 Sutton, S. R. *et al.* Vanadium K edge XANES of synthetic and natural basaltic glasses and application to microscale oxygen barometry. *Geochim. Cosmochim. Acta* **69**, 2333-2348 (2005).
32 Hanawalt, J. D., Rinn, H. W. & Frevel, L. K. Chemical Analysis by X-Ray Diffraction. *Industrial & Engineering Chemistry Analytical Edition* **10**, 457-512 (1938).
33 Bouloux, J.-C., Milosevic, I. & Galy, J. Les hypovanadates de magnésium MgVO3 et MgV2O5. Structure cristalline de MgVO3. *J. Solid State Chem.* **16**, 393-398 (1976).

Associated Content

Supporting information

Acknowledgements

This work was supported as part of the Joint Center for Energy Storage Research (JCESR), an Energy Innovation Hub funded by the U.S. Department of Energy, Office of Science, Basic Energy Sciences. This research used resources at the Electron Microscopy Center in the Center for Nanoscale Materials and the Advanced Photon Source (beamline 11-ID-C and 20-BM-B), two

U.S. Department of Energy (DOE) Office of Science User Facilities operated for the DOE Office of Science by Argonne National Laboratory under Contract No. DE-AC02-06CH11357. The Materials Project (BES DOE Grant No. EDCBEE) is acknowledged for the simulation support.

Author contributions

Sa, N. and Burrell, A. K. designed the experiment. Sa, N., Proffit, D. L. and Vaughey, J. T. synthesized the cathode materials. Fister T. T., Sun C. and Zhenxing Feng helped with the XANES measurements. Lipson, A. L. and Sa, N. performed and analyzed SEM and EDX data. Liu, M. SaiGautam, G., Persson, K. and Ceder, G. performed and advised the computation work. Ren. Y., Fenter, P. A. performed and discussed the diffraction data. Liao, C. helped with the conductivity measurement. Hanh, N. and Zavadil K. R. contributed to the discussion of the electrolyte development.

Additional information

Supplementary Information for this paper can be found at

http://www.nature.com/naturecommunications

Competing financial interests: the authors declare no competing financial interests.

Reprints and permission: information is available online